

Self-Trapping of Light and Nonlinear Localized Modes in 2D Photonic Crystals and Waveguides

Serge F. M. Ingaleev ^{1,2} and Yuri S. Kivshar ¹

¹ Nonlinear Physics Group, Research School of Physical Sciences and Engineering
Australian National University, Canberra ACT 0200, Australia

² Bogolyubov Institute for Theoretical Physics, Kiev 03143, Ukraine

1 Introduction

Photonic crystals are usually viewed as an optical analog of semiconductors that modify the properties of light similar to a microscopic atomic lattice that creates a semiconductor band-gap for electrons [1]. It is therefore believed that by replacing relatively slow electrons with photons as the carriers of information, the speed and bandwidth of advanced communication systems will be dramatically increased, thus revolutionizing the telecommunications industry. Recent fabrication of photonic crystals with a band gap at optical wavelengths from 1.35 μm to 1.95 μm makes this promise very realistic [2].

To employ the high-tech potential of photonic crystals, it is crucially important to achieve a dynamical tunability of their band gap [3]. This idea can be realized by changing the light intensity in the so-called nonlinear photonic crystals, having a periodic modulation of the nonlinear refractive index [4]. Exploration of nonlinear properties of photonic band-gap (PBG) materials is an important direction of research that opens new applications of photonic crystals for all-optical signal processing and switching, allowing an effective way to create tunable band-gap structures operating entirely with light.

One of the important physical concepts associated with nonlinearity is the energy self-trapping and localization. In the linear physics, the idea of localization is always associated with disorder that breaks translational invariance. However, during the recent years it was demonstrated that localization can occur in the absence of any disorder and solely due to nonlinearity in the form of intrinsic localized modes [5]. A rigorous proof of the existence of time-periodic, spatially localized solutions describing such nonlinear modes has been presented for a broad class of Hamiltonian coupled-oscillator nonlinear lattices [6], but approximate analytical solutions can also be found in many other cases, demonstrating a generality of the concept of nonlinear localized modes.

Nonlinear localized modes can be easily identified in numerical molecular-dynamics simulations in many different physical models (see, e.g., Ref. [5] for a review), but only very recently the first experimental observations of spatially localized nonlinear modes have been reported in mixed-valence tran-

sition in metal complexes [7], quasi-one-dimensional antiferromagnetic chains [8], and arrays of Josephson junctions [9]. Importantly, very similar types of spatially localized nonlinear modes have been experimentally observed in macroscopic mechanical [10] and guided-wave optical [11] systems.

Recent experimental observations of nonlinear localized modes, as well as numerous theoretical results, indicate that nonlinearity-induced localization and spatially localized modes can be expected in physical systems of very different nature. From the viewpoint of possible practical applications, self-localized states in optics seem to be the most promising ones; they can lead to different types of nonlinear all-optical switching devices where light manipulates and controls light itself by varying the input intensity. As a result, the study of nonlinear localized modes in photonic structures is expected to bring a variety of realistic applications of intrinsic localized modes.

One of the promising fields where the concept of nonlinear localized modes may find practical applications is the physics of photonic crystals [or photonic band gap (PBG) materials] {periodic dielectric structures that produce many of the same phenomena for photons as the crystalline atomic potential does for electrons [1]. Three-dimensional (3D) photonic crystals for visible light have been successfully fabricated only within the past year or two, and presently many research groups are working on creating tunable band-gap switches and transistors operating entirely with light. The most recent idea is to employ nonlinear properties of band-gap materials, thus creating nonlinear photonic crystals including those where nonlinear susceptibility is periodic as well [4,12].

Nonlinear photonic crystals (or photonic crystals with embedded nonlinear inclusions) create an ideal environment for the generation and observation of nonlinear localized photonic modes. In particular, the existence of such modes for the frequencies in the photonic band gaps has been predicted [13] for 2D and 3D photonic crystals with Kerr nonlinearity. Nonlinear localized modes can be also excited at nonlinear interfaces with quadratic nonlinearity [14], or along dielectric waveguide structures possessing a nonlinear Kerr-type response [15].

In this Chapter, we study selftrapping of light and nonlinear localized modes in nonlinear photonic crystals and photonic crystal waveguides. For simplicity, we consider the case of a 2D photonic crystal with embedded nonlinear rods (inclusions) and demonstrate that the effective interaction in such a nonlinear waveguide structure is nonlocal (see also Ref. [16]), so that the nonlinear effects can be described by a nontrivial generalization of the nonlinear lattice models that include the long-range coupling and nonlocal nonlinearity. We describe several different types of nonlinear guided-wave states in photonic crystal waveguides and analyse their properties. Also, we predict the existence of nonlinear localized modes (highly localized modes analogous to gap solitons in the continuum limit) in symmetry-reduced nonlinear photonic crystals.

2 Basic Equations

Let us consider a 2D photonic crystal created by a periodic lattice of parallel, infinitely long dielectric rods in air (see Fig. 1). We assume that the rods are parallel to the x_3 axis, so that the system is characterized by the dielectric constant $\epsilon(x) = \epsilon(x_1; x_2)$. As is well known [1], the photonic crystals of this type can possess a complete band gap for the E-polarized (with the electric field $E \parallel x_3$) light propagating in the $(x_1; x_2)$ -plane. The evolution of such a light is governed by the scalar wave equation

$$r^2 E(x; t) - \frac{1}{c^2} \partial_t^2 [\epsilon(x) E] = 0; \quad (1)$$

where $r^2 = \partial_{x_1}^2 + \partial_{x_2}^2$ and E is the x_3 component of E . Taking the electric field in the form

$$E(x; t) = e^{i\omega t} E(x; t; j);$$

where $E(x; t; j)$ is a slowly varying envelope, i.e. $\partial_t^2 E(x; t; j) \ll \partial_t E(x; t; j)$, Eq. (1) reduces to

$$r^2 + \epsilon(x) - \frac{1}{c^2} E(x; t; j)' - 2i\epsilon(x) \frac{1}{c^2} \frac{\partial E}{\partial t} = 0; \quad (2)$$

In the stationary case, i.e. when the r.h.s. of Eq. (2) vanishes, this equation describes an eigenvalue problem which can be solved, e.g. by the plane waves method [17], in the case of a perfect photonic crystal, for which the dielectric constant $\epsilon(x) = \epsilon_p(x)$ is a periodic function defined as

$$\epsilon_p(x + s_{ij}) = \epsilon_p(x); \quad (3)$$

where i and j are arbitrary integers, and

$$s_{ij} = ia_1 + ja_2 \quad (4)$$

is a linear combination of the lattice vectors a_1 and a_2 .

For definiteness, we consider the 2D photonic crystal earlier analyses (in the linear limit) in Refs. [18,19]. That is, we assume that cylindrical rods with radius $r_0 = 0.18a$ and dielectric constant $\epsilon_0 = 11.56$ form a square lattice with the distance a between two neighboring rods, so that $a_1 = ax_1$ and $a_2 = ax_2$. The frequency band structure for this type of 2D photonic crystal is shown in Fig. 1 where, using the notations of the solid-state physics, the wave dispersion is mapped onto the Brillouin zone of the so-called reciprocal lattice that faces are known as Γ , M , and X . As follows from Fig. 1, there exists a large (38%) band gap that extends from the lower cut-off frequency, $\omega = 0.302 \times 2\pi/c = 0.443 \times 2\pi/c$, to the upper band-gap frequency, $\omega = 0.443 \times 2\pi/c$. If the frequency of a low-intensity light falls into the band gap, the light cannot propagate through the photonic crystal and is reflected.

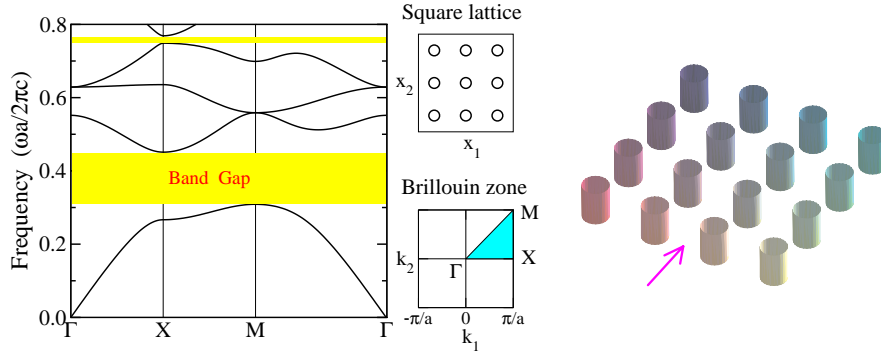


Fig. 1. The band-gap structure of the photonic crystal consisting of a square lattice of dielectric rods with $r_0 = 0.18a$ and $\epsilon_0 = 11.56$ (the band gaps are shaded). The top center inset shows a cross-sectional view of the 2D photonic crystal depicted in the right inset. The bottom center inset shows the corresponding Brillouin zone, with the irreducible zone shaded.

3 Effect Modes: The Green's Function Approach

One of the most intriguing properties of photonic band gap crystals is the emergence of exponentially localized modes that may appear within the photonic band gaps when a defect is embedded into an otherwise perfect photonic crystal. The simplest way to create a defect in a 2D photonic crystal is to introduce an additional defect rod with the radius r_d and the dielectric constant $\epsilon_d(x)$. In this case, the dielectric constant $\epsilon(x)$ can be presented as a sum of periodic and defect-induced terms, i.e.

$$\epsilon(x) = \epsilon_p(x) + \epsilon_d(x);$$

and, therefore, Eq. (2) takes the form

$$r^2 + \frac{!}{c}^2 \epsilon_p(x) E(x; t; j!) = \hat{L} E(x; t; j!); \quad (5)$$

where the operator

$$\hat{L} = \frac{!}{c}^2 \epsilon_d(x) + 2i\epsilon(x) \frac{!}{c^2} \frac{\partial}{\partial t} \quad (6)$$

is introduced for convenience. Equation (5) can also be written in the equivalent integral form

$$E(x; t; j!) = -d^2 y G(x; y; j!) \hat{L} E(y; t; j!); \quad (7)$$

where $G(x; y; j!)$ is the Green's function defined, in a standard way, as a solution of the equation

$$r^2 + \frac{!}{c}^2 \epsilon_p(x) G(x; y; j!) = \delta(x - y); \quad (8)$$

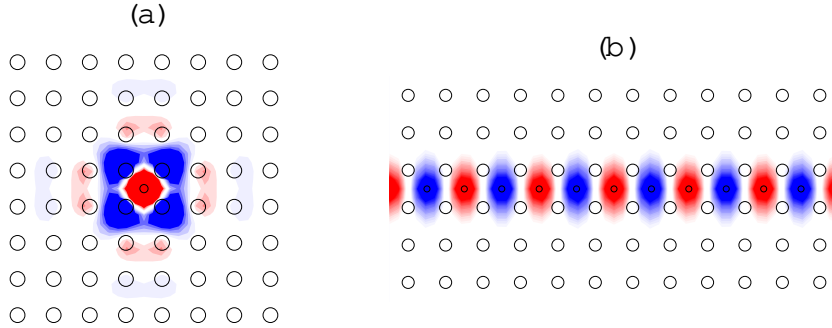


Fig. 2. Electric field of the linear modes localized (a) around a single defect rod and (b) in a waveguide created by an array of the defect rods. The rod positions are indicated by circles and the amplitude of the electric field is indicated by color (red, for positive values, and blue, for negative values).

Properties of the Green function of a perfect 2D photonic crystal are described in more details in Ref. [17]. Here, we notice that the Green function is symmetric, i.e.

$$G(x; y; j!) = G(y; x; j!)$$

and periodic, i.e.

$$G(x + s_{ij}; y + s_{ij}; j!) = G(x; y; j!);$$

where s_{ij} is defined by Eq. (4).

The Green's function can be calculated by means of the Fourier transform

$$G(x; y; j!) = \frac{1}{Z_1} \int_0^{\infty} dt e^{i\omega t} G(x; y; t) \quad (9)$$

applied to the time-dependent Green's function governed by the equation

$$r^2 \nabla_p^2 G(x; y; t) = -i\omega(t) (x - y); \quad (10)$$

which has been solved by the finite-difference time-domain method [20].

Now that we have calculated the Green's function, we can figure out the defect states solving Eq. (7) directly. For example, Fig. 2 (a) shows a defect mode created by introducing a single defect rod with the radius $r_d = 0.1a$ and dielectric constant $\epsilon_d = 11.56$ into the 2D photonic crystal shown in Fig. 1.

A simple solid-state-physics analogy helps to make a giant step towards photonic applications creating waveguides as arrays of defect rods. In conventional waveguides such as optical fibers, light is confined by total internal reflection due to the difference in the refractive indices of the waveguide core and cladding. The waveguides based on the PBG materials employ a different

physical mechanism: the guidance is due to a surrounding band gap structure that supports a mode that is in the band gap and is forbidden from propagating in a bulk because of the gap, in the way a defect mode is created. That is, photonic waveguides operate in a manner similar to resonant cavities.

The simplest photonic-crystal waveguide can be created by a straight line of defect rods, as shown in Fig. 2(b). Instead of a single localized state of an isolated defect, a waveguide supports propagating states (guided modes) with the frequencies in a narrow band located inside the band gap of a perfect crystal. Such guided modes have a periodical profile along the waveguide, and they decay exponentially in the transverse direction, see Fig. 2(b).

One of the weaknesses of conventional optical waveguides based on the concern due to a total internal reflection is that creating bends is difficult. Unless the radius of the bend is large compared to the wavelength, much of the light will be lost. This is a serious problem in creating "integrated optical circuits", since the space required for large-radius bends is unavailable. Since the physical principles for the operation of photonic crystals are different, when a bend is created in the waveguide, the light remains trapped and the only possible problem is that of reflection. However, it is still possible to get almost 100% transmission, as was recently demonstrated numerically [18,19] and also verified experimentally [21,22].

4 Nonlinear Waveguides in 2D Photonic Crystals

In this Section, we follow the results of Ref. [16] and describe the properties of nonlinear photonic crystal waveguides created by inserting an additional row of rods made from a Kerr-type nonlinear material characterized by the third-order nonlinear susceptibility $\chi^{(3)}$ and the linear dielectric constant $\epsilon_d^{(0)}$. For definiteness, we assume that $\epsilon_d^{(0)} = \epsilon_0 = 11.56$. As we show below, changing the radius r_d of these defect rods and their location within the crystal, one can create nonlinear waveguides with quite different properties.

4.1 Effective 1D discrete nonlinear equation

Let us assume that the nonlinear defect rods embedded into the photonic crystal along a selected direction s_{ij} are located at the points $x_m = x_0 + m s_{ij}$. In this case, the correction to the dielectric constant is

$$\epsilon_d(x) = \epsilon_d^{(0)} + \sum_m \chi^{(3)} \delta(x - x_m); \quad (11)$$

where

$$\delta(x) = \begin{cases} 1; & \text{for } |x - x_m| \leq r_d; \\ 0; & \text{for } |x - x_m| > r_d; \end{cases} \quad (12)$$

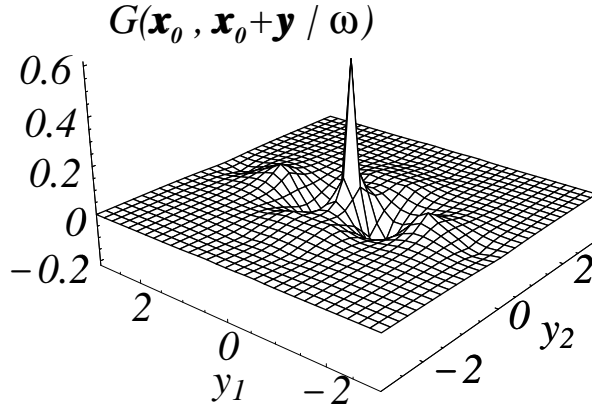


Fig. 3. The Green function $G(x_0; x_0 + y/\omega)$ for the photonic crystal shown in Fig. 1 ($x_0 = a_1 = 2$ and $\omega = 0.33/2 \approx a$).

The second term in Eq. (11) takes into account a contribution due to the Kerr nonlinearity (we assume that the electric field is scaled with the nonlinear susceptibility, ⁽³⁾).

If the radius of the defect rods r_d is sufficiently small, the electric field $E(x; t; j)$ inside them is almost constant and one can derive, by substituting Eq. (11) into Eq. (7) and averaging over of the cross-section of the rods [15], an approximate discrete nonlinear equation

$$i \frac{\partial}{\partial t} E_n - E_n + \sum_m^X J_{n,m}(\omega) (E_d^{(0)} + E_m)^2 E_m = 0; \quad (13)$$

for the amplitudes of the electric field $E_n(t; j)$ — $E(x_n; t; j)$ inside the defect rods. The parameter and the coupling constants

$$J_n(\omega) = \frac{1}{c} \sum_{r_d}^Z d^2 y G(x_0; x_n + y; j) \quad (14)$$

are determined by Green's function $G(x; y; j)$ of the perfect photonic crystal.

Based on this equation, we provide a systematic analysis of different types of nonlinear localized modes. In particular, it is possible to show [16] that the approximation of the nearest-neighbor interaction is very crude in many of the cases analyses. Since the effective coupling coefficients are defined by the Green's function, this can be seen directly from Fig. 3 that shows a typical spatial profile of the Green's function which, in general, characterizes a long-range interaction, very typical for photonic crystals. As a consequence of that, the coupling coefficients $J_n(\omega)$ calculated from Eq. (14) decrease slowly with

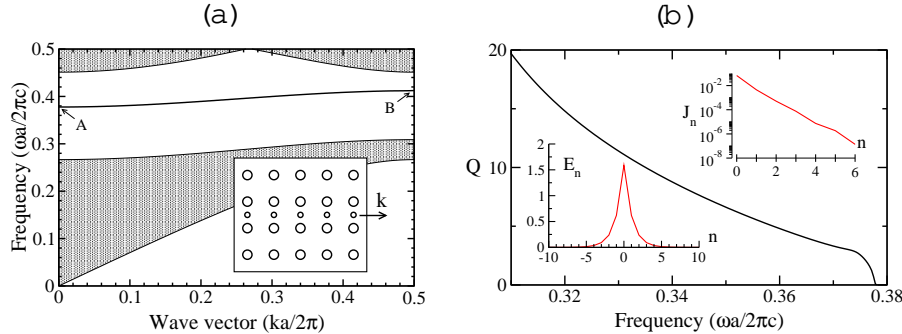


Fig. 4. (a) Dispersion relation for the photonic crystal waveguide shown in the inset ($\epsilon_0 = \epsilon_d = 11.56$, $r_0 = 0.18a$, $r_d = 0.10a$). The grey areas are the projected band structure of the perfect 2D photonic crystal. The frequencies at the indicated points are: $\omega_A = 0.378 \text{ } 2 \text{ } c/a$ and $\omega_B = 0.412 \text{ } 2 \text{ } c/a$. (b) Mode power $Q (|J|)$ of the nonlinear mode excited in the corresponding photonic crystal waveguide. The right inset gives the dependence $J_n (|J|)$ calculated at $\omega = 0.37 \text{ } 2 \text{ } c/a$. The left inset presents the profile of the corresponding nonlinear localized mode.

the site number n . For s_{01} and s_{10} directions, the coupling coefficients can be approximated by an exponential function as follows

$$J_n (\omega) = \begin{cases} J_0 (\omega) & \text{for } n = 0; \\ J_0 (\omega) e^{-(\omega - \omega_0)/\gamma} & \text{for } n \neq 0; \end{cases}$$

where the characteristic decay rate γ can be as small as 0.85, depending on the values of ω_0 , x_0 , and r_d , and it can be even smaller for other types of photonic crystals (with different r_0 and ϵ_0).

This result allows us to draw an analogy between the problem under consideration and a class of the nonlinear Schrödinger (NLS) equations that describe nonlinear excitations in quasi-one-dimensional molecular chains with long-range (e.g. dipole-dipole) interaction between the particles and local-on-site nonlinearities [23,24]. For such systems, it was shown that the effect of nonlocal interparticle interaction introduces some new features in the properties of nonlinear localized modes (in particular, bistability in their spectrum). Moreover, for our model the coupling coefficients $J_n (\omega)$ can be either unstructured and monotonically decaying, i.e. $J_n (\omega) = J_n (\omega)$, or staggered and oscillating from site to site, i.e. $J_n (\omega) = (-1)^n J_n (\omega)$. We therefore expect that effective nonlocality in both linear and nonlinear terms of Eq. (13) will bring a number of new features into the properties of nonlinear localized modes excited in the photonic crystal waveguides.

4.2 Staggered and unstructured localized modes

As can be seen from the structure of the Green's function presented in Fig. 3, the case of monotonically varying coefficients $J_n (\omega)$ can occur for the wave-

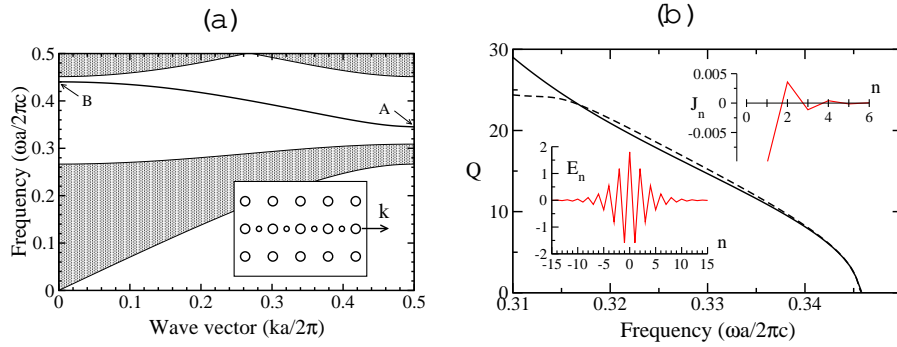


Fig. 5. (a) Dispersion relation for the photonic crystal waveguide shown in the inset ($n_0 = n_d = 11.56$, $r_0 = 0.18a$, $r_d = 0.10a$). The grey areas are the projected band structure of the perfect 2D photonic crystal. The frequencies at the indicated points are: $\omega_A = 0.346 \text{ } 2 \text{ } c/a$ and $\omega_B = 0.440 \text{ } 2 \text{ } c/a$. (b) Mode power Q (!) of the nonlinear mode excited in the corresponding photonic crystal waveguide. Two cases are presented: the case of nonlinear rods in a linear photonic crystal (solid line) and the case of a completely nonlinear photonic crystal (dashed line). The right inset shows the behavior of the coupling coefficients J_n (!) for $n = 1$ ($J_0 = 0.045$) at $\omega = 0.33 \text{ } 2 \text{ } c/a$. The left inset shows the profile of the nonlinear mode.

uide oriented in the s_{01} direction with $x_0 = a_1 = 2$. In this case, the frequency of a linear guided mode, that can be excited in such a waveguide, takes a minimum value at $k = 0$ [see Fig. 4(a)], and the corresponding nonlinear mode is expected to be untaggered.

We have solved Eq. (13) numerically and found that nonlinearity can lead to the existence of guided modes localized in both directions, i.e. in the direction perpendicular to the waveguide, due to the guiding properties of a channel waveguide created by defect rods, and in the direction of the waveguide, due to the nonlinearity-induced self-trapping effect. Such nonlinear modes exist with the frequencies below the frequency of the linear guided mode of the waveguide, i.e. below the frequency ω_A in Fig. 4(a), and are indeed untaggered, with the bell-shaped profile along the waveguide direction shown in the left inset of Fig. 4(b).

The 2D nonlinear modes localized in both dimensions can be characterized by the mode power which we define, by analogy with the NLS equation, as

$$Q = \sum_n |E_n|^2 : \quad (15)$$

This power is closely related to the energy of the electric field in the 2D photonic crystal accumulated in the nonlinear mode. In Fig. 4(b) we plot the dependence of Q on frequency, for the waveguide geometry shown in Fig. 4(a).

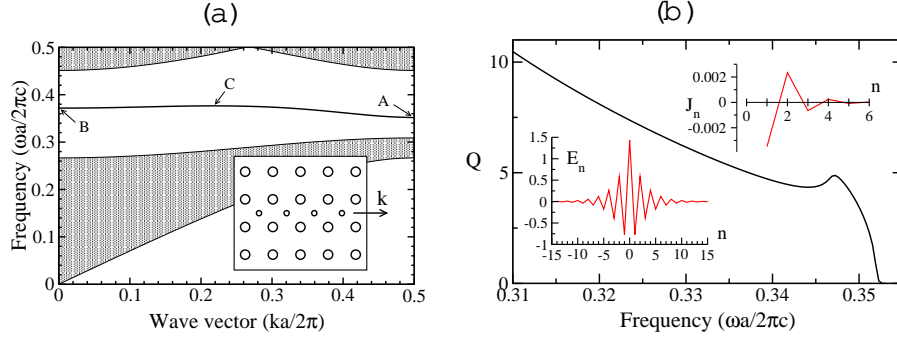


Fig. 6. (a) Dispersion relation for the photonic crystal waveguide shown in the inset ($\epsilon_0 = \epsilon_d = 11.56$, $r_0 = 0.18a$, $r_d = 0.10a$). The grey areas are the projected band structure of the perfect 2D photonic crystal. The frequencies at the indicated points are: $\omega_A = 0.352 \cdot 2 \pi a$, $\omega_B = 0.371 \cdot 2 \pi a$, and $\omega_C = 0.376 \cdot 2 \pi a$ (at $k = 0.217 \cdot 2 \pi a$). (b) Mode power $Q(\omega)$ of the nonlinear mode excited in the corresponding photonic crystal waveguide. The right inset shows the behavior of the coupling coefficients $J_n(\omega)$ for $n = 1$ ($J_0 = 0.068$) at $\omega = 0.345 \cdot 2 \pi a$. The left inset shows the profile of the corresponding nonlinear mode.

As can be seen from the Green's function shown in Fig. 3, the case of staggered coupling coefficients $J_n(\omega)$ can be obtained for the waveguide oriented in the s_{10} direction with $x_0 = a_1/2$. In this case, the frequency dependence of the linear guided mode of the waveguide takes the minimum at $k = \pi/a$ [see Fig. 5(a)]. Accordingly, the nonlinear guided mode localized along the direction of the waveguide is expected to exist with the frequency below the lowest frequency ω_A of the linear guided mode, with a staggered profile. The longitudinal profile of such a 2D nonlinear localized mode is shown in the left inset in Fig. 5(b), together with the dependence of the mode power Q on the frequency (solid curve), which in this case is again monotonic.

The results presented above are obtained for linear photonic crystals with nonlinear waveguides created by a row of defect rods. However, we have carried out the same analysis for the general case of a nonlinear photonic crystal that is created by rods of different size but made of the same nonlinear material. Importantly, we have found relatively small difference in all the results presented above provided nonlinearity is weak. In particular, for the photonic crystal waveguide shown in Fig. 5(a), the results for linear and nonlinear photonic crystals are very close. Indeed, for the mode power Q the results corresponding to a nonlinear photonic crystal are shown in Fig. 5(b) by a dashed curve, and for $Q < 20$ this curve almost coincides with the solid curve corresponding to the case of a nonlinear waveguide embedded into a 2D linear photonic crystal.

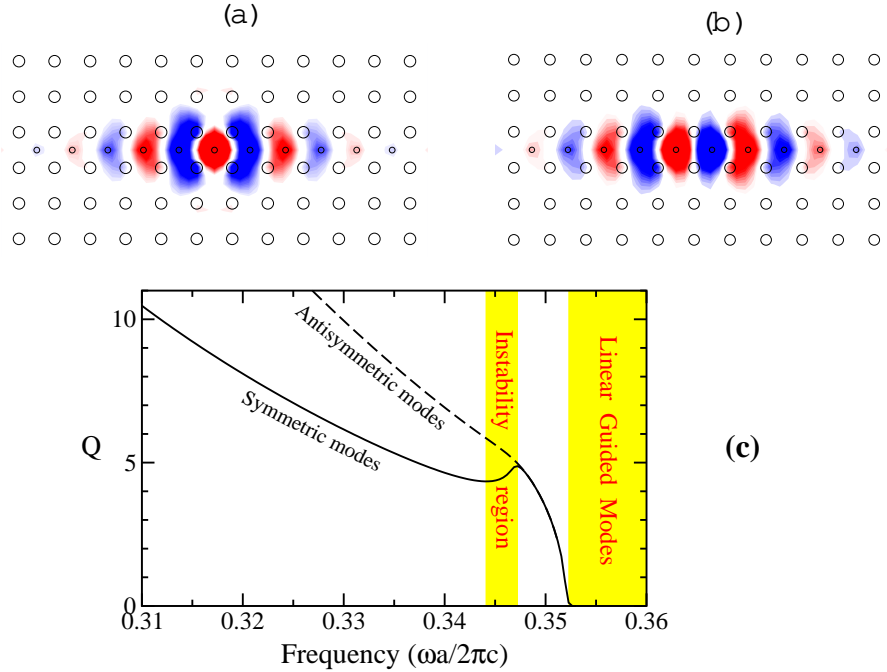


Fig. 7. Examples of the (a) symmetric and (b) antisymmetric localized modes. The rod positions are indicated by circles and the amplitude of the electric field is indicated by color [red, for positive values, and blue, for negative values]; (c) Power Q vs. frequency dependencies calculated for two modes of different symmetry in the photonic crystal waveguide shown in Fig. 6.

4.3 Instability of nonlinear localized modes

Let us now consider the waveguide created by a row of defect rods which are located at the points $x_0 = (a_1 + a_2)/2$, along a straight line in either the s_{10} or s_{01} directions. The results for this case are presented in Figs. 6{7. The coupling coefficients J_n are described by a slowly decaying staggered function of the site number n , so that the effective interaction decays on the scale larger than in the two cases considered above.

It is remarkable that, similar to the NLS models with long-ranged dispersive interactions [23,24], we find a non-monotonic behavior of the mode power Q (!) for this type of nonlinear photonic crystal waveguides: specifically, Q (!) increases in the frequency interval $0.344 < (! a=2 c) < 0.347$ [shaded in Fig. 7(c)]. One can expect that, similar to the results earlier obtained for the nonlocal NLS models [23,24], the nonlinear localized modes in this interval are unstable and will eventually decay or transform into the modes of higher or lower frequency [25]. What counts is that there is an interval of mode power in which two stable nonlinear localized modes of different widths do

coexist. Since the mode power is closely related to the mode energy, one can expect that the mode energy is also non-monotonic function of λ . Such a phenomenon is known as **bistability**, and in the problem under consideration it occurs as a direct manifestation of the nonlocality of the effective (linear and nonlinear) interaction between the defect rod sites.

Being interested in the mobility of the nonlinear localized modes we investigated, in addition to the symmetric modes shown in the left inset in Fig. 6(b) and in Fig. 7(a), also the antisymmetric localized modes shown in Fig. 7(b). Our calculations show that the power $Q(\lambda)$ of the antisymmetric modes always (for all values of λ and all types of waveguides) exceeds that for symmetric ones [see, e.g., Fig. 7(c)]. Thus, antisymmetric modes are expected to be unstable and they should decay or transform into a lower-energy symmetric modes. In fact, the difference between power of antisymmetric and symmetric modes determines the Peierls-Nabarro barrier which characterizes the mobility of nonlinear localized modes in discrete systems. One can see in Fig. 7(c) that the Peierls-Nabarro barrier is negligible for $0.347 < |\lambda|/a = 2c/a < 0.352$ and thus such localized modes should be mobile. However, the Peierls-Nabarro barrier becomes significantly large for highly localized modes with $|\lambda| < 0.344 - 2c/a$ and, as a consequence, such modes should be immobile. Hence, the bistability phenomenon in the photonic crystal waveguides of the type depicted in Figs. 6-7 opens up fresh opportunities [24] for switching between immobile localized modes (used for energy storage) and mobile localized modes (used for energy transport).

5 Self-Trapping of Light in a Reduced-Symmetric 2D Nonlinear Photonic Crystal

In this Section we study the properties of nonlinear localized modes in a 2D photonic crystal composed of two types of circular rods: the rods of radius r_0 made from a linear dielectric material and placed at the corners of a square lattice with the lattice spacing a , and the rods of radius r_d made from a nonlinear dielectric material and placed at the center of each unit cell (see right inset in Fig. 8). Recently, such photonic crystals of reduced symmetry have attracted considerable interest because of their ability to possess larger absolute band gaps [26]. The band-gap structure of the reduced-symmetry photonic crystal is shown in Fig. 8. As is seen, it possesses two band gaps, first of which extends from $|\lambda| = 0.426 - 2c/a$ to $|\lambda| = 0.453 - 2c/a$.

A low-intensity light cannot propagate through a photonic crystal if the light frequency falls into a band gap. However, it has been recently suggested [13] that in the case of a 2D periodic medium with a Kerr-type nonlinear material, high-intensity light with frequency inside the gap can propagate in the form of finite energy solitary waves (2D gap solitons). These solitary waves were found to be stable [13], but the conclusion was based on the coupled-mode equations valid for a weak modulation of the dielectric constant " χ ".

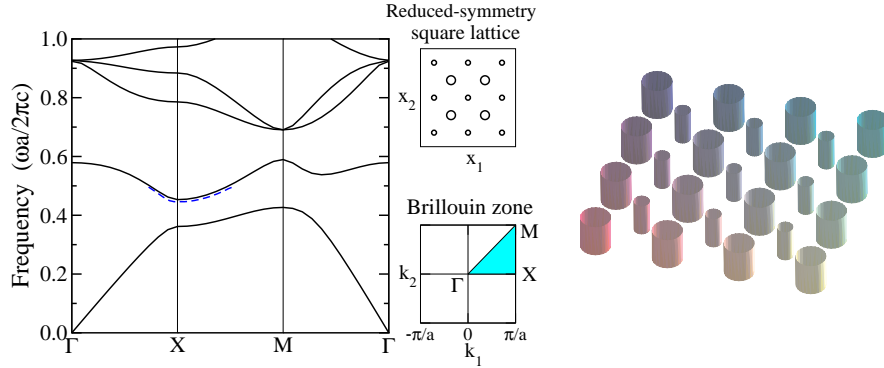


Fig. 8. Band-gap structure of the reduced-symmetry photonic crystal with $r_0 = 0.1a$, $r_d = 0.05a$, and $\epsilon = 11.4$ for both types of rods. Full lines are calculated by the MIT Photonic-Bands program [27] whereas dashed line is found from the effective discrete model. The top center inset shows a cross-sectional view of the 2D photonic crystal depicted in the right inset. The bottom center inset shows the corresponding Brillouin zone.

However, in real photonic crystals the modulation of $\epsilon(x)$ is comparable to its average value. Thus, the results of Ref. [13] have a limited applicability to the properties of localized modes in realistic photonic crystals.

More specifically, the coupled-mode equations are valid if and only if the band gap is vanishingly small, i.e. A^2 where A is an effective amplitude of the mode, that is a small parameter in the multi-scale asymptotic expansions [28]. If we apply this model to describe nonlinear modes in a wider gap (see, e.g., discussions in Ref. [28]), we obtain a 2D nonlinear Schrödinger (NLS) equation known to possess no stable localized solutions. Moreover, the 2D localized modes described by the coupled-mode equations are expected to possess an oscillatory instability recently discovered for a broad class of coupled-mode Thirring-like equations [29]. Thus, it is clear that, if nonlinear localized modes do exist in realistic PBG materials, their stability should be associated with different physical mechanisms not accounted for by simplified continuum models.

5.1 Effective 2D discrete nonlinear equation

The reduced-symmetry "diatomic" photonic crystal shown in Fig. 8 can be considered as a square lattice of the "nonlinear defect rods" of small radius r_d ($r_d < r_0$) embedded into the ordinary single-rod photonic crystal formed by a square lattice of rods of larger radius r_0 in air.

The positions of the defect rods can then be described by the radius-vector $\mathbf{x}_{n,m} = n \mathbf{a}_1 + m \mathbf{a}_2$, where \mathbf{a}_1 and \mathbf{a}_2 are the primitive lattice vectors of the 2D photonic crystal, while n and m are arbitrary integers. For our model, we

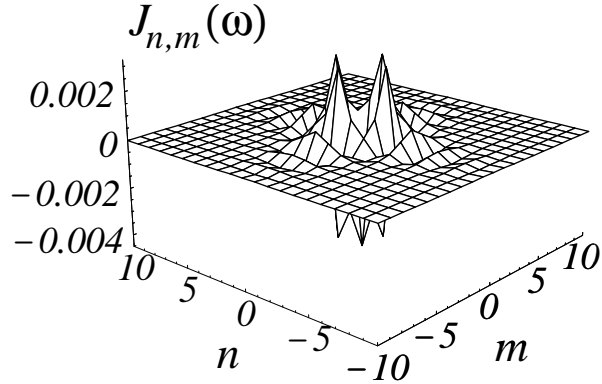


Fig. 9. Coupling coefficients $J_{n,m}(\omega)$ for the photonic crystal depicted in Fig. 8 (the contribution of the coefficient $J_{0,0} = 0.039$ is not shown). The frequency $\omega = 0.4456$ falls into the first band gap.

take

$$u_d(x) = \sum_{n,m}^{n,m} u_d^{(0)} + \mathcal{E}(x; t; j!) \sum_{n,m}^{\infty} (x - x_{n,m}); \quad (16)$$

where (x) is defined by Eq. (12). In the same way as we derived the model (13), one can obtain an approximate 2D discrete nonlinear equation

$$i \frac{\partial}{\partial t} E_{n,m} - E_{n,m} + \sum_{k,l}^{\infty} J_{n-k,m-l}(\omega) (u_d^{(0)} + \mathcal{E}_{k,l} j!) E_{k,l} = 0; \quad (17)$$

for the amplitudes of the electric field $E_{n,m}(t; j!)$ $\mathcal{E}(x_{n,m}; t; j!)$ inside the defect rods. Again, the parameter and the coupling constants

$$J_{n,m}(\omega) = \frac{1}{c} \sum_{r_d}^Z d^2 y G(x_0, y; x_{n,m} + y j!); \quad (18)$$

are determined by Green's function $G(x; y j!)$ of the single-rod photonic crystal defined in Eq. (8).

As we discussed in the previous section, the Green's function $G(x; y j!)$ and, consequently, the coupling coefficients $J_{n,m}(\omega)$ are usually highly long-ranged functions. For instance, to reach accurate results for the photonic crystal depicted in Fig. 8 one should take into account the interaction between at least 10 neighbors (see Fig. 9). By this means, Eq. (17) is a nontrivial long-range generalization of a 2D discrete NLS equation extensively studied during the last decade [30]. We have checked the accuracy of the approximation provided by Eq. (17) solving it in the linear limit, in order to find the band-gap structure associated with linear stationary mode. The low-frequency part of

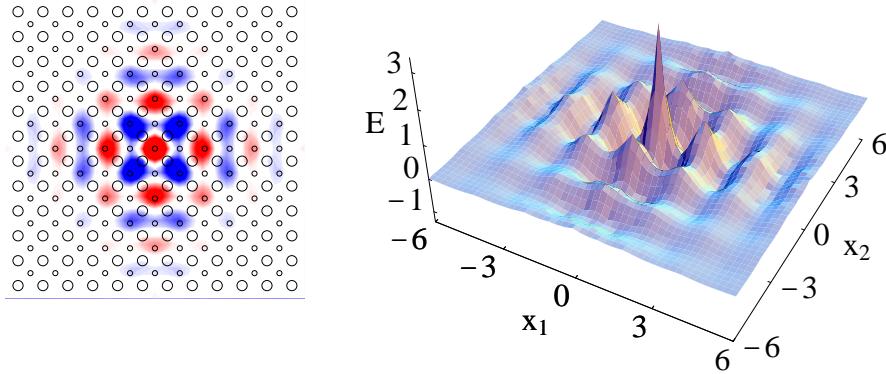


Fig. 10. Top (left) and 3D (right) views of a nonlinear localized mode in the first band gap of 2D photonic crystal depicted in Fig. 8.

this dependence is depicted in Fig. 8 by a dashed line, with a minimum at $\omega = 0.446 \text{ rad/s}$. One can see that the frequencies of the linear modes calculated from Eq. (17) are in a good agreement with those calculated directly from Eq. (2). It lends a support to the validity of Eq. (17) and allows us to use it for studying nonlinear properties.

5.2 Nonlinear 2D localized modes

Stationary nonlinear modes described by Eq. (17) are found numerically by the Newton-Raphson iteration scheme. We reveal the existence of a continuous family of such modes, and a typical example [smoothed by continuous optimization for Eq. (5)] of nonlinear localized mode is shown in Fig. 10. Besides Hamiltonian, Eq. (17) conserves the mode power defined as

$$Q(\omega) = \sum_{n,m}^X |E_{n,m}|^2; \quad (19)$$

which is proportional to the energy of the electric field accumulated in the nonlinear localized modes. In Fig. 11, we plot the dependence of the mode power Q on the frequency ω for the photonic crystal shown in Fig. 8. As we have already discussed, this dependence represents a very important characteristic of nonlinear localized modes which allows to determine their stability by means of the Vakhitov-Kolokolov stability criterion: $dQ/d\omega > 0$ for unstable modes (this criterion has been extended to 2D NLS models in [31]).

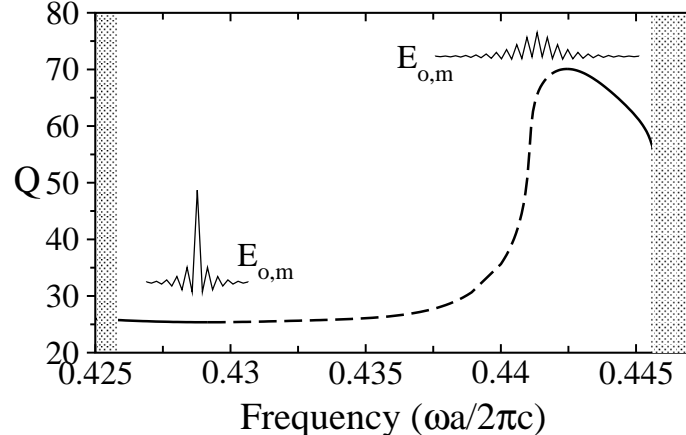


Fig. 11. Power Q of the nonlinear localized mode vs. its frequency for the 2D photonic crystal shown in Fig. 8. Solid lines correspond to stable modes whereas dashed line indicates the interval of instability (with $dQ/d\omega > 0$). The grey areas show the projected band structure of the crystal. Insets show typical profiles of stable modes.

As is well known (see, e.g., Refs. [31,32]), in the unbounded 2D NLS equation with linear dispersive interactions the only high-amplitude intrinsically localized modes are stable. One can see from Fig. 11 that such high-amplitude modes are also stable in the case of the photonic crystal under consideration. However, to excite these modes one should use the light beam of unreasonably high intensity (for the medium nonlinear dielectrics with relatively small nonlinear susceptibility ⁽³⁾). Usually the low-amplitude modes in 2D NLS models are unstable and either collapse or decay [30]. In fact, they can be stabilized by some external forces (e.g., due to interactions with boundaries or disorder [33]), but in this case the excitations are pinned and cannot be used for energy or signal transfer.

Here we show that, in a sharp contrast to the 2D discrete NLS models discussed earlier, the low-amplitude modes of Eq. (17) can be stabilized due to the presence of nonlinear long-range dispersion in this equation. For instance, as is seen from Fig. 11, the low-amplitude modes of the photonic crystal being considered in Fig. 8 are stable. It should be emphasized that such stabilization does not occur in the models with only linear long-range dispersion [30]. In order to gain a better insight into the stabilization mechanism, we have carried out the studies of Eq. (17) for the exponentially decaying coupling coefficients $J_{n,m}$. Our results reveal that the most important factor which determines stability of the low-amplitude modes is the ratio of the coupling coefficients at the local nonlinearity ($J_{0,0}$) and the nonlinear dispersion ($J_{0,1}$). If the coupling coefficients $J_{n,m}$ decrease with the distances n and m rapidly, the low-amplitude modes are essentially stable for $J_{0,0}=J_{0,1}$. 13. However, this

estimation is usually lowered because the stabilization is favored by the presence of long-range interactions. Since the discussed stabilization mechanism of low-amplitude modes preserves the translational symmetry of the system, such modes are expected to be mobile.

It should be emphasized that the stabilization of low-amplitude modes is not inherent to all types of nonlinear photonic crystals. On the contrary, the photonic crystals must be carefully designed to support stable low-amplitude modes. For example, in the photonic crystal with $r_1 = 0.18a$ and $r_2 = 0.10a$ the ratio $J_{0,0}/J_{0,1}$ exceeds 18 and such modes are always unstable.

6 Concluding Remarks

Exploration of nonlinear properties of PBG materials may open new important application of photonic crystals for all-optical signal processing and switching, allowing an effective way to create tunable band-gap structures operating entirely with light. Nonlinear photonic crystals, and nonlinear waveguides created in the photonic structures with a periodically modulated dielectric constant, create an ideal environment for the generation and observation of nonlinear localized modes.

As follows from our results, nonlinear localized modes can be excited in photonic crystal waveguides of different geometry. For several geometries of 2D waveguides, we have demonstrated that such modes are described by a new type of nonlinear lattice modes that include long-range interaction and effectively nonlocal nonlinear response. It is expected that the general features of nonlinear guided modes described here will be preserved in other types of photonic crystal waveguides. Additionally, similar types of nonlinear localized modes are expected in photonic crystal fibers [34] consisting of a periodic air-hole lattice that runs along the length of the fiber, provided the fiber core is made of a highly nonlinear material (see, e.g., Ref. [35]).

Experimental observation of nonlinear photonic localized modes would require not only the use of photonic materials with a relatively large nonlinear refractive index (such as AlGaAs waveguide PBG structures [36] or polymer PBG crystals [37]), but also a control of the group-velocity dispersion and band-gap parameters. The latter can be achieved by employing the surface coupling technique [38] that is able to provide coupling to specific points of the dispersion curve, opening up a very straightforward way to access nonlinear effects.

Acknowledgments

The authors are indebted to K. Busch, A. M. Gurn, and C. Soukoulis for encouraging comments, and R. Sammut for useful collaboration and support. Sergey M. Ingaleev is thankful to Yu B. Gaididei for productive discussions. The

work has been partially supported by the Planning and Performance Fund of the Institute of Advanced Studies.

References

1. J.D. Joannopoulos, R.B. Meade, and J.N. Winn, *Photonic Crystals: Molding the Flow of Light* (Princeton University Press, Princeton N.J., 1995).
2. J.G. Fleming and S.-Y. Lin, *Opt. Lett.* **24**, 49 (1999).
3. See, e.g., K. Busch and S. John, *Phys. Rev. Lett.* **83**, 967 (1999), and discussions therein.
4. V. Berger, *Phys. Rev. Lett.* **81**, 4136 (1998); and also the recent experiment: N.G.R. Broderick, G.W. Ross, H.L.O. Erhuis, D.J. Richardson, and D.C. Hanna, *Phys. Rev. Lett.* **84**, 4345 (2000); S. Saltiel and Yu.S. Kivshar, *Opt. Lett.* **25**, 1204 (2000).
5. See, e.g., S. Flach and C.R.W. Ellis, *Phys. Rep.* **295**, 181 (1998); O.M. Braun and Yu.S. Kivshar, *Phys. Rep.* **306**, 1 (1998), Chap. 6.
6. R.S. Mackay and S. Aubry, *Nonlinearity* **7**, 1623 (1994); see also S. Aubry, *Physica D* **103**, 201 (1997).
7. B.I. Swanson, J.A. Brozik, S.P. Love, G.F. Strouse, A.P. Shreve, A.R.Bishop, W.Z. Wang, and M.I. Salkola, *Phys. Rev. Lett.* **82**, 3288 (1999).
8. U.T. Schwarz, L.Q. English, and A.J. Sievers, *Phys. Rev. Lett.* **83**, 223 (1999).
9. E. Trias, J.J. Mazon, and T.P. Orlando, *Phys. Rev. Lett.* **84**, 741 (2000); P. Binder, D. Abramov, A.V. Ustinov, S. Flach, and Y. Zolotaryuk, *Phys. Rev. Lett.* **84**, 745 (2000).
10. F.M. Russel, Y. Zolotaryuk, and J.C. Eilbeck, *Phys. Rev. B* **55**, 6304 (1997).
11. H.S. Eisenberg, Y. Silberberg, R. Marandotti, A.R. Boyd, and J.S. Aitchison, *Phys. Rev. Lett.* **81**, 3383 (1998).
12. A.A. Sukhorukov, Yu.S. Kivshar, O. Bang, J. Martorell, J. Trull, and R. Vilaseca, *Optics and Photonics News* **10** (12) 34 (1999).
13. S. John and N.A. Kozbek, *Phys. Rev. Lett.* **71**, 1168 (1993); *Phys. Rev. E* **57**, 2287 (1998).
14. A.A. Sukhorukov, Yu.S. Kivshar, and O. Bang, *Phys. Rev. E* **60**, R41 (1999).
15. A.R.M. oGum, *Phys. Lett. A* **251**, 322 (1999); *Phys. Lett. A* **260**, 314 (1999).
16. S.F. M. Ingaleev, Yu.S. Kivshar, and R.A. Sammut, *Phys. Rev. E* **62**, 5777 (2000).
17. A.A. Maradudin and A.R.M. oGum, in *Photonic Band Gaps and Localization*, NATO ASI Series B: Physics, Vol. 308, Ed. C.M. Soukoulis (Plenum Press, New York, 1993), p. 247.
18. A. Melik, J.C. Chen, I. Kurland, S. Fan, P.R. Villeneuve, and J.D. Joannopoulos, *Phys. Rev. Lett.* **77**, 3787 (1996).
19. A. Melik, S. Fan, and J.D. Joannopoulos, *Phys. Rev. B* **58**, 4809 (1998).
20. A.J. Ward and J.B. Pendry, *Phys. Rev. B* **58**, 7252 (1998).
21. S.-Y. Lin, E. Chow, V. Hietala, P.R. Villeneuve, and J.D. Joannopoulos, *Science* **282**, 274 (1998).
22. M. Tokushima, H. Kosaka, A. Tomita, and H. Yamada, *Appl. Phys. Lett.* **76**, 952 (2000).
23. Y.B. Gaididei, S.F. M. Ingaleev, P.L. Christiansen, and K. Rasmussen, *Phys. Rev. E* **55**, 6141 (1997).

24. M. Johansson, Y. B. Gaididei, P. L. Christiansen, and K. Rasmussen, *Phys. Rev. E* **57**, 4739 (1998).
25. See, e.g., the examples for the continuous generalised NLS models, D. E. Pelinovsky, V. V. Afanas'ev, and Yu. S. Kivshar, *Phys. Rev. E* **53**, 1940 (1996).
26. C. M. Anderson and K. P. Gaididei, *Phys. Rev. Lett.* **77**, 2949 (1996); *Phys. Rev. B* **56**, 7313 (1997).
27. S. G. Johnson, <http://ab-initio.mit.edu/mpb/>
28. Yu. S. Kivshar, O. A. Chubykalo, O. V. Usatenko, and D. V. Grin'yan, *Int. J. Mod. Phys. B* **9**, 2963 (1995).
29. I. V. Barashenkov, D. E. Pelinovsky, and E. V. Zemlyanaya, *Phys. Rev. Lett.* **80**, 5117 (1998); A. De Rossi, C. Conti, and S. Trillo, *Phys. Rev. Lett.* **81**, 85 (1998).
30. See, e.g., V. K. Mezentsev, S. L. Musher, I. V. Ryzhenkova, and S. K. Turitsyn, *JETP Lett.* **60**, 829 (1994); S. Flach, K. Kladko, and R. S. Mackay, *Phys. Rev. Lett.* **78**, 1207 (1997); P. L. Christiansen et al., *Phys. Rev. B* **57**, 11303 (1998).
31. E. W. Laedke et al., *JETP Lett.* **62**, 677 (1995).
32. E. W. Laedke, K. H. Spatschek, S. K. Turitsyn, and V. K. Mezentsev, *Phys. Rev. E* **52**, 5549 (1995); Yu. B. Gaididei, P. L. Christiansen, K. Rasmussen, and M. Johansson, *Phys. Rev. B* **55**, R13365 (1997).
33. Yu. B. Gaididei, D. H. Endriksen, P. L. Christiansen, and K. Rasmussen, *Phys. Rev. B* **58**, 3075 (1998).
34. T. A. Birks, J. C. Knight, and P. St. J. Russell, *Opt. Lett.* **22**, 961 (1997).
35. B. J. Eggleton, P. S. Westbrook, R. S. Windeler, S. Spalter, and T. A. Strasser, *Opt. Lett.* **24**, 1460 (1999).
36. P. Millar et al., *Opt. Lett.* **24**, 685 (1999); A. A. Heimy et al., *Opt. Lett.* **25**, 1370 (2000).
37. S. Shoji and S. Kawata, *Appl. Phys. Lett.* **76**, 2668 (2000).
38. V. N. Astratov et al., *Phys. Rev. B* **60**, R16255 (1999).